Canadian Mineralogist
Vol. 22, pp. 281-295 (1984)

AMPHIBOLE AND PYROXENE DEVELOPMENT IN FENITE FROM CANTLEY, QUEBEC*

DONALD D. HOGARTH

Ottawa-Carleton Centre for Geoscience Studies, University of Ottawa, Ottawa, Ontario K1N 6N5

PIERRE LAPOINTE

Earth Physics Branch, Department of Energy, Mines and Resources, Ottawa, Ontario K1A 0Y3

ABSTRACT

Proterozoic fenites near Cantley, Quebec, formed from biotite gneiss and hypersthene–augite gneiss by metasomatism possibly related to carbonatite, are characterized by magnesio-arfvedsonite, magnesio-riebeckite and aegirine. The ratio $Ca/(Ca+Na+K)$ decreases from older to younger pyriboles. In magnesio-arfvedsonite, the ratio $Fe_T/(Fe_T+Mg)$ first increases and then decreases, but K remains constant with respect to Na and Ca. Magnesio-riebeckite, replacing cummingtonite or hypersthene, shows a trend similar to that of magnesio-arfvedsonite but is notably depleted in K and F. In magnesio-arfvedsonite, and possibly magnesio-riebeckite, the *A* sites are progressively filled. Na-amphibole and Na-pyroxene, in the same hand specimen, are approximately coeval. Early aegirine substitutes for the hedenbergite end-member, and later aegirine, for the diopside end-member. Late aegirine is contemporaneous with major growth of (Fe, Ti) oxides. Na-pyriboles from open systems, such as those of the Cantley fenite, tend to define curves on chemical variation diagrams, whereas those from closed systems tend to cluster; those formed in either system, but from protoliths of different chemical compositions, give random plots.

Keywords: fenite, magnesio-arfvedsonite, magnesio-riebeckite, aegirine, carbonatite, metasomatic rocks, chemical trends, oxidation, Cantley, Ottawa – Bonnechère graben, Quebec.

SOMMAIRE

Les fénites d'âge protérozoïque de la région de Cantley (Québec) ont été formées à partir d'un gneiss à biotite et hypersthène – augite par un métasomatisme qui serait relié à une carbonatite. Elles sont caractérisées par la présence de magnésio-arfvedsonite, magnésio-riebeckite et aegyrine. Dans les pyriboles, le rapport $Ca/(Ca+Na+K)$ décroît des plus anciennes aux plus récentes. Dans la magnésio-arfvedsonite, le rapport $Fe_T/(Fe_T+Mg)$ croît d'abord et puis diminue; par contre, le rapport $K/(Na+Ca)$ reste constant. La magnésio-riebeckite, qui remplace soit la cummingtonite, soit l'hypersthène, se comporte comme la magnésio-arfvedsonite sauf appauvrissement notable en K et F. Dans la magnésio-arfvedsonite et peut-être la magnésio-riebeckite, l'occupation des sites *A* se fait de façon croissante. L'amphibole et le pyroxène sodiques d'un même échantillon sont à peu près contemporains. L'aegyrine précoce remplace l'hédenbergite, l'aegyrine tardive, le diopside. L'aegyrine tardive se développe lors de la croissance des oxydes de fer et de titane. Les pyriboles sodiques qui évoluent dans un système ouvert tels ceux des fénites de Cantley, définissent des courbes dans les diagrammes de variation chimique; par contre, ceux d'un système clos ont tendance à se grouper, et ceux qui proviennent de protolithes de composition chimique variable montrent, indépendamment du système, une distribution aléatoire.

Mots-clés: fénite, magnésio-arfvedsonite, magnésio-riebeickite, aegyrine, métasomatisme, variations chimiques, oxydation, graben Ottawa – Bonnechère, Québec.

INTRODUCTION

The chemical trends illustrated by Na-amphibole and Na-pyroxene from fenite have not been clearly defined. Attempts have been made to outline these trends in a general way (*e.g.*, Sutherland 1969, Vartiainen & Woolley 1976), but these were not entirely successful, in part owing to lack of care in sample selection and impure mineral separates. In order to define fenitic pyribole trends more precisely we will describe these minerals from a small area that shows minimal variation in the protolith. We will also compare these pyriboles with those of three other nonigneous occurrences, each with a distinct origin. In this paper the term *pyribole* is used to refer collectively to pyroxene and amphibole.

An area near Cantley, Quebec (Fig. 1) where fenite replaces various Precambrian rocks was chosen for this research. Occurrences were selected from two metasomatized protoliths: biotite gneiss and hypersthene–augite gneiss. Fenite, "the Mg–Fe–Na silicate zone" in Figures 1 and 2, is delineated by the presence of Na-amphibole and Na-pyroxene based on field observations. Sample selection was based on representative mineral associations and the suitability of grains for microprobe and petrographic examination.

The fenites in this area were described briefly by Hogarth & Moore (1972) and Hogarth (1977). Further details are to be found in the thesis of Lapointe (1979) and the regional report of Hogarth (1981). The associated oxides have been described by Cockburn (1966). This research is part of an ongoing study at the University of Ottawa on the geology of the Gatineau–Lièvre district.

*Publication 05–84 of the Ottawa–Carleton Centre for Geoscience Studies.

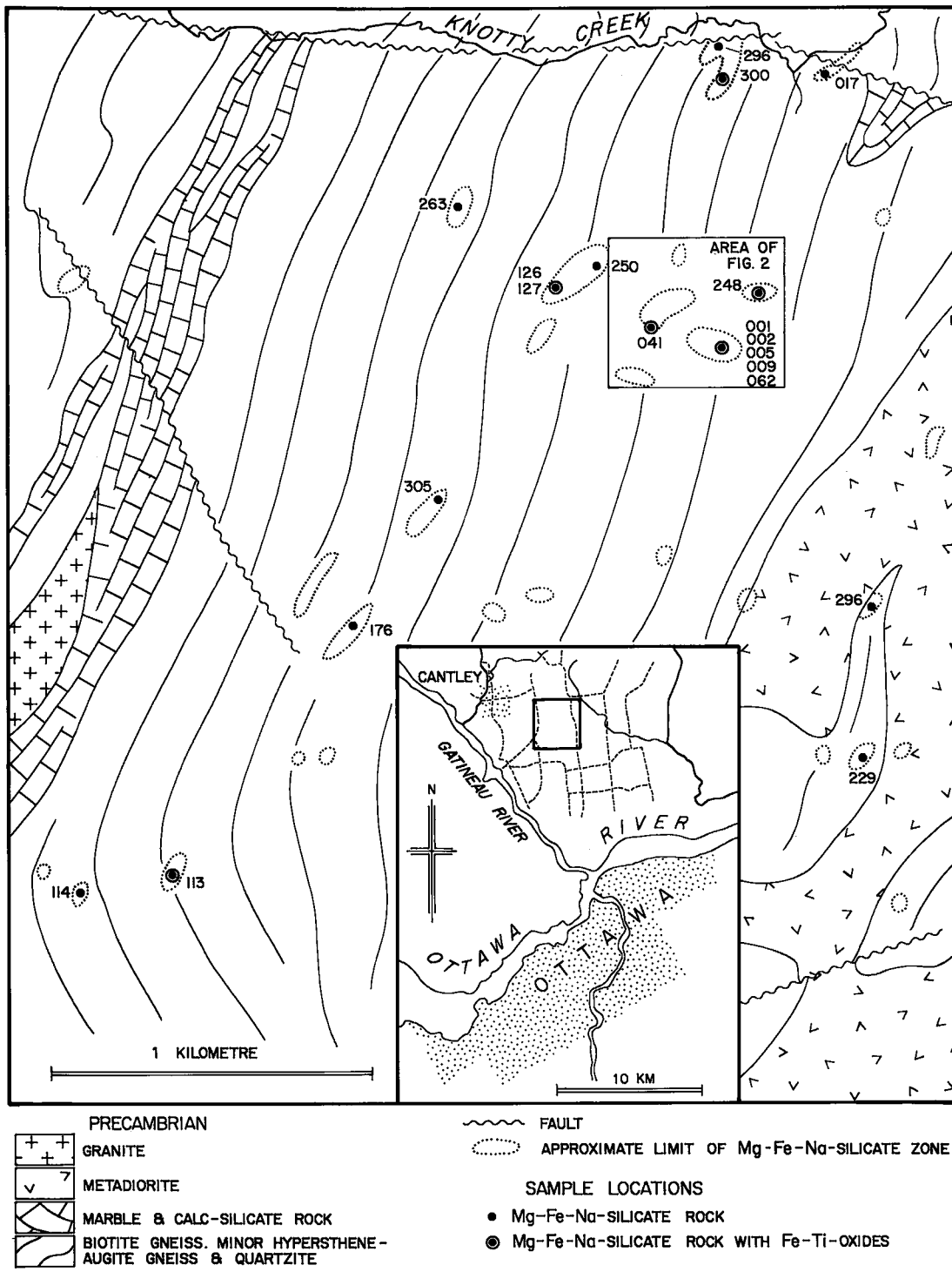

FIG. 1. Map showing location and geology of study area (generalized after Hogarth 1981) and sample locations. Limits of the Mg–Fe–Na zone mark the field-observed disappearance of Na-amphibole and Na-pyroxene.

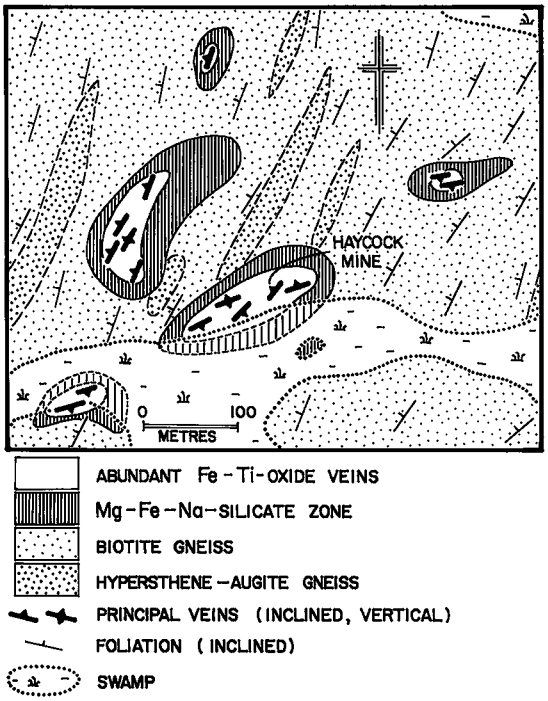

FIG. 2. Detailed geology of the Haycock Mine and vicinity. Location is given by rectangle on Figure 1.

GEOLOGY

The map area lies on the western flank of an almost isoclinal synform, overturned toward the east and plunging northward. Within this synform, the principal rocks define a high-grade metamorphic suite belonging to the Grenville Supergroup. The ascending sequence is graphitic marble and granite orthogneiss (left-hand side, Fig. 1), a thin layer of quartzite (omitted for simplicity), biotite gneiss and minor interlayered quartzofeldspathic and hypersthene–augite gneisses (centre of area) and, finally, a non-graphitic marble and metadiorite (right-hand side, Fig. 1). Neither "granite" (granite to granodiorite) nor "metadiorite" (quartz diorite to diorite) show cross-cutting relationships with surrounding rocks. They are concordantly foliated near their margins and display an igneous texture (porphyritic and ophitic, respectively) in their cores. All rock types are cut by small dykes of granite pegmatite. Gneisses have attained the granulite metamorphic facies, indicated by the associations hypersthene + augite + andesine, hypersthene + almandine + andesine, hypersthene + K-feldspar and sillimanite + cordierite + K-feldspar. However, retrograde activity has been extensive and is characterized by such alteration products as cummingtonite, saponite and biotite after hyperstene, hornblende and biotite after augite, chlorite after biotite, and sericite and scapolite after plagioclase. In addition, the monoclinic K-feldspar has inverted to microcline.

Numerous bodies of fenite, the largest 2500 m long and 150 m wide, are situated in a belt that approximately parallels the regional foliation. This belt attains a maximum thickness of 4 km near Cantley, whence it can be traced northeasterly for 22 km to an occurrence near the Lièvre River. The fenite replaces or transects all the above rock types and is superimposed on both the unaltered and retrograde minerals.

A "silicate assemblage" characterizes most of the specimens listed in Table 1. It is composed of major amounts of Na-pyribole, lesser albite and substantial quantities of phlogopite. Associated minerals are disseminated hematite and minor but typical calcite, barite and apatite. It appears as patches, disseminations and cross-cutting veinlets. Indisputable replacement-textures, such as aegirine pseudomorphs (and partial pseudomorphs) after biotite, were observed in several thin sections.

Coarse-grained oxides of iron and titanium (the "oxide assemblage") are present in cross-cutting veins and lenses of specularite–rutile–magnetite (*e.g.*, specimen 127, Table 1), veinlets of specularite–calcite–barite, and strike fracture-fillings of specularite–rutile–apatite (*e.g.*, specimen 002, Table 1). The surrounding rock is largely replaced with the silicate assemblage. Cross-cutting lenses, the largest 3.5 m across, were tested for iron ore in the 1870s (the Haycock mine: Cirkel 1909). Commonly, the oxide veins and lenses are most abundant in the core of an occurrence; the comparatively oxide-free silicate assemblage characterizes the envelope (Fig. 2).

Two Ca–Ba–*REE* carbonatites, associated with fenite, crop out on the west side of the synform (north of Fig. 1) and on the east side (northeast of Fig. 1), and are possibly the source of metasomatic solutions that formed the fenites. With the exception of three small syenite dykes on the east flank of the synform (3 km east of the centre of Fig. 1), no alkaline intrusive rock is known in the immediate area.

The age of the fenite can be tentatively placed in the interval 850 to 1050 Ma. The Cantley fenite postdates granite pegmatite but probably is older than the K/Ar ages determined from phlogopite separated from fenite at the Haycock mine (980 ± 52 Ma, M. Shafiqullah, pers. comm.; 862 ± 31 Ma, Wanless *et al.* 1974, p. 64, age G.S.C. 72–88).

Northwest-, northeast- and east–west-striking faults cut the metamorphic rocks, but their relationship to granite pegmatite, syenite, carbonatite and

TABLE 1. MODAL COMPOSITION OF FENITE SPECIMENS

	001	002	009	041	062	113	114	126	127	176	229	248	250	263	296	300	305
Na-pyroxene	27.4	<1	40.8	1.6	17.6	14.7	13.0	8.7	Tr	7.5	5.0	13.2	0.3	6.2	8.3	14.4	18.2
Na-amphibole	19.2	0	13.3	0	2.6	3.9	11.9	6.4	0	5.1	7.3	16.3	6.0	8.5	13.6	21.9	2.7
Phlogopite & biotite	4.9	20	Tr	16.3	25.1	1.3	8.4	16.7	<1	10.4	21.0	1.9	7.6	13.0	3.2	1.9	0.9
Fresh albite	11.6	0	3.4	3.5	Tr	6.6	2.0	10.9	0	Tr	6.2	1.3	Tr	Tr	16.9	1.5	0.2
Fe, Ti oxides	3.5	50	6.7	6.4	2.6	3.5	3.6	1.8	90	3.9	3.6	4.0	4.9	1.2	3.1	8.6	2.1
Calcite	3.6	10	9.1	0.3	6.8	7.0	0.1	9.8	0	Tr	5.6	3.2	0.6	0.2	6.6	4.8	1.9
Barite	0.5	<1	0.7	0.2	0	1.1	0.1	1.7	0	0.1	1.1	Tr	Tr	0	0.6	1.2	0.1
Apatite	1.6	20	1.2	0.9	0.4	0.1	0.1	0.4	0.1	0.3	0.5	0.2	0.2	0.2	0.1	0.2	1.0
Altered feldspars	27.4	0	24.1	70.7	44.9	46.0	60.7	43.7	Tr	66.0	47.4	59.8	73.3	58.6	41.6	31.9	72.9
Quartz	0	0		Tr	0	11.4	Tr	0	10	6.5	1.9	0.1	0.9	5.4	2.1	13.5	0.1
Remainder	0.4	0	0.7	0.1	0	4.4	0.1	0	0	0.2	0.4	0	6.2	6.7	3.9	0	0
Assemblage	Ct	Ox	Ct	Ct	Sil	Sil	Sil	Sil	Ox	Sil	Sil	Sil	Sil	Sil	Sil	Sil	Sil

Abbreviations: Ox oxide; Ct silicate assemblage < 1 m from oxide zone; Sil silicate assemblage; Tr trace.

fenite is not definitely known. Possibly they are part of the Ottawa - Bonnechère graben system, which has periodically been active since Helikian time (Hogarth & Moore 1972).

The Cantley area is on the north side of the Ottawa - Bonnechère graben; this structure has possibly been important in localizing carbonatite and fenite. Alkalic activity associated with the graben is generally Phanerozoic (Gittins *et al.* 1967), but Proterozoic representatives are also known. Thus fenite near Meach Lake, Quebec, 15 km west of the present map-area, was dated at 910 and 930 Ma (phlogopite, K/Ar; Hogarth 1966) and silicocarbonatite near the Ottawa River, 80 km northwest of the map area, at 1050 Ma (zircon, U/Pb; Lumbers 1982).

Methods of Investigation

Pyriboles from 15 polished thin sections (those of Table 1, excepting specimens 001 and 009) were analyzed by Hogarth at the Smithsonian Institution with an ARL - SEMQ microprobe operating with a specimen current of 30 nA and an accelerating voltage of 15 kV. For unzoned grains, averages of several (up to 8) grains per section were recorded; for zoned grains, values for the core and rim of a grain were recorded separately. Data were corrected by the methods of Bence & Albee (1968) and Albee & Ray (1970). Analytical data are believed to be accurate to within 2% of the value recorded for major oxides (SiO_2, FeO_T, MgO), 5% for Na_2O, 10% for minor oxides (TiO_2, Al_2O_3, Cr_2O_3, MnO, CaO, K_2O) and 20% for F. Pyriboles from specimens 001 and 009 were analyzed for Lapointe by Tariq Ahmedali at McGill University with an Acton microprobe, operated at 15 kV and 30 nA. Data were reduced with the EMPADR program (Rucklidge & Gasparrini 1969).

Amphibole from one specimen (017) was separated and then analyzed by Lapointe by atomic absorption. Ferrous iron was determined by titration (Jen 1973). Pyroxene in two other specimens (005 and 006) was handpicked and analyzed by E.L.P. Mercy. Separate 005 came from a late calcite–pyroxene veinlet cutting coarse-grained oxides at the Haycock mine; separate 006 came from a calcite–pyroxene–rutile vein cutting fenite near Little Dam Lake, approximately 13 km north-northeast of the Haycock mine.

The second author carried out Mössbauer analysis of pyriboles taken from approximately the same location as specimen 062 (Fig. 1).

Mineralogy

General features

Na-amphiboles and Na-pyroxene are easily distinguished in the field. The pyroxene (aegirine) is yellow green, the Na-amphiboles are pale blue-green (magnesio-arfvedsonite) or blue to violet (magnesio-riebeckite). The minerals commonly "diffuse out" from veinlets or are restricted to certain layers in the original rock. Some amphiboles are asbestiform, but normally the grains are short to long prismatic. Only in veins that cut the oxide assemblage are relatively large crystals of Na-pyroxene (up to 2 mm across) found.

The paragenesis can be studied readily in thin section. In some silicate assemblages, the earliest alkalic pyribole appears to be a Na-amphibole, which grows at the expense of quartz (clustered around edges and interstitially), biotite (on the rims and along cleavages) and, more rarely, cummingtonite (on rims and in zones within crystal packets) and feldspar (irregular patches). This early-formed amphibole (Fig. 3) is commonly transected or replaced by fine-grained pyroxene. In other cases (Fig. 4), the amphibole appears to postdate pyroxene. Rarely, early and late amphiboles occur together in the same thin section. However, in the majority of specimens studied,

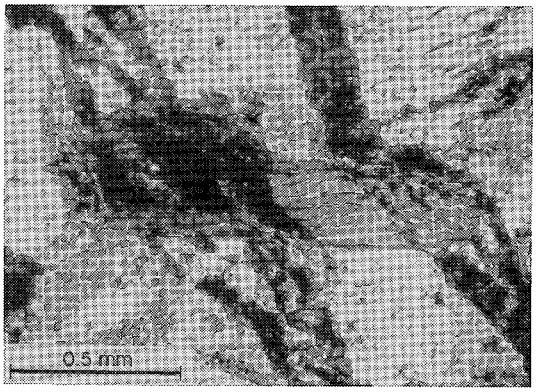

FIG. 3. Aegirine veinlet (almost black) in microcline (grey-white) deflected and cutting through a subparallel, fibrous aggregate of magnesio-arfvedsonite (medium grey). Plane-polarized light, thin section 114.

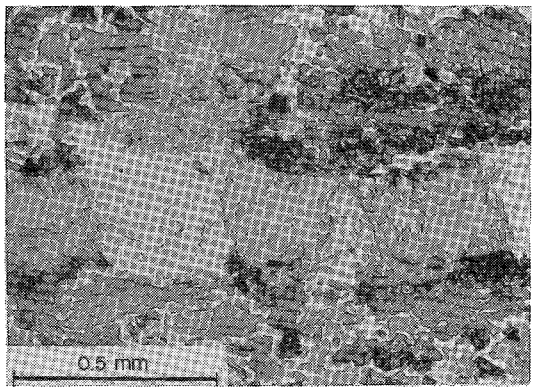

FIG. 4. Veinlet of albite (almost white) and magnesio-riebeckite (grey) transecting a polygranular cluster of aegirine (dark grey, right-hand side of photograph) in microcline–albite–phlogopite rock. Plane-polarized light, thin section 062.

pyroxene and amphibole seem roughly coeval. One mineral abuts against the other without obvious replacement or reaction relationship.

A notable feature in several specimens is the preference of one mineral for a particular host. The Na-pyroxene preferentially replaces quartz, rarely replaces feldspar, and does not replace actinolite or cummingtonite. An extreme example, illustrated by specimen 114, shows quartz and biotite + perthite well segregated into alternating layers in a finely laminated gneiss. Amphibole has preferentially replaced part of the feldspar, whereas pyroxene has replaced the quartz. Possibly the control here is chemical, with K freely entering the structure of an amphibole, but being excluded from that of a pyroxene.

Amphibole

Compositions of the amphiboles and their formulae are presented in Table 2. The proportion of Fe^{2+} and Fe^{3+} is calculated on the basis of 13 octahedral + tetrahedral ions and 46 charges. This calculation stipulates complete absence of vacancies in the *M*1, *M*2 and *M*3 structural positions.

Amphiboles of three distinct types have been found in the silicate assemblage (IMA nomenclature; Leake 1978). Magnesio-arfvedsonite is the most abundant, but some specimens (017,062) contain magnesio-riebeckite. Besides having less Na and more Fe^{3+}, the latter is notably depleted in K and F. One specimen (250; Fig. 5) contains cummingtonite (250*b*) partly replaced by magnesio-riebeckite (250*a*).

Some grains are conspicuously zoned (Table 2), with a narrow rim (*r*) grading into the main core-zone (*c*). Composition 114*r* is from the inky blue tip of a tapered crystal, 114*c* represents its almost colorless core. The rim is lower in Ca, but F does not vary. Amphibole 296 shows minor zoning in the same sense. Amphibole 062 shows no evidence of chemical zoning, but optical measurements ($Z\Lambda c$) suggest that here too, the core is richer in Ca than the rim, although some other, undetermined variable may have influenced optical properties.

Potassium is an important constituent of magnesio-arfvedsonite, reaching nearly 3% K_2O in specimen 300. Whereas this percentage is indeed unusual, elsewhere magnesio-arfvedsonite from fenite commonly exceeds 2% K_2O. Al is minor and cannot be correlated with Ca. Mn and Ti are insignificant (< 0.50% MnO and TiO_2).

Pyroxene

Compositions of pyroxene are presented in Table 3. The proportion of Fe^{2+} to Fe^{3+} has been calculated assuming 4 cations with a total of 12 positive charges. Aegirine compositions predominate but 263 and 305 extend into the field of aegirine-augite (Fe^{3+} < 0.8 ions per 6 oxygen atoms), according to the definition of Deer *et al.* (1978, p. 483). However, in this paper we will refer to all our specimens as aegirine, for convenience.

As with amphiboles, some crystals are distinctly zoned. In Table 3, core compositions are denoted by *c* and rim compositions, by *r*. In all cases, the core is richer in Ca than the rim, in agreement with optical properties (larger $X\Lambda c$, smaller birefringence). Ti and Al are irregularly distributed with respect to Ca; Mn is minor (< 0.20% MnO).

Chemical trends in the pyribole suite

The Cantley pyriboles define smooth curves on variation diagrams. Thus the 17 amphibole compositions can be fitted to two nearly parallel curves on

TABLE 2. CHEMICAL COMPOSITION OF AMPHIBOLE

	001	009	017	062	113	114o	114r	126	176	229	248	250a	250b	263	296o	296r	300	305
SiO_2	57.08	56.04	55.15	54.72	55.24	55.67	55.53	54.34	54.86	55.08	54.92	54.72	54.79	54.76	54.71	54.33	54.87	56.09
TiO_2	0.10	0.12	n.a.	0.49	0.16	0.05	0.05	0.18	0.27	0.21	0.09	0.29	0.11	0.16	0.19	0.17	0.10	0.10
Al_2O_3	0.44	0.45	1.14	1.00	1.25	0.57	0.58	2.05	1.60	1.31	0.88	0.29	0.46	1.77	1.29	1.52	0.86	1.20
Fe_2O_3	5.89	5.71	13.60	14.41	11.25	10.49	13.53	10.86	10.59	12.39	11.62	15.99	-----	12.19	11.23	11.39	9.52	10.96
FeO	4.96	5.64	8.24	6.44	2.85	1.50	0.72	2.29	3.00	1.39	1.39	5.73	19.62	1.62	3.06	2.98	1.43	1.42
MnO	n.a.	n.a.	0.14	0.09	0.19	0.41	0.45	0.13	0.19	0.12	0.18	0.06	0.31	0.23	0.18	0.15	0.24	0.15
MgO	16.75	16.30	10.04	10.99	16.32	17.71	16.80	16.56	16.36	16.72	17.07	11.51	21.39	16.54	15.92	15.82	17.58	17.41
CaO	0.52	0.34	2.23	0.42	1.19	1.97	1.08	1.09	1.40	1.97	0.93	0.11	0.49	1.68	1.57	1.32	0.76	3.10
Na_2O	8.71	9.06	5.43	6.85	8.60	8.08	8.19	8.58	8.51	7.45	8.61	7.51	0.49	7.96	7.98	8.27	8.32	6.77
K_2O	2.41	2.38	0.28	0.37	1.50	1.64	1.60	2.10	1.58	1.55	1.86	0.28	0.19	1.58	1.49	1.48	2.94	1.14
F	n.a.	n.a.	n.a.	0.7	3.3	2.6	2.8	2.4	1.9	2.1	2.3	0.3	0.1	2.1	2.4	2.5	2.7	1.3
	96.86	96.04	96.25	96.48	101.85	100.69	101.33	100.58	100.26	100.29	99.85	96.79	97.95	100.59	100.02	99.93	99.32	99.64
O=F	-----	-----	-----	0.3	1.4	1.1	1.2	1.0	0.8	0.9	1.0	0.1	.04	0.9	1.0	1.1	1.1	0.55
Total	96.86	96.04	96.25	96.18	100.45	99.59	100.13	99.58	99.46	99.39	98.85	96.69	97.91	99.69	99.02	98.83	98.22	99.09
Ions based on 13 (T + C) cations and 46 positive charges; (250b on 46 positive charges and all iron assumed FeO).																		
Si	8.135	8.097	8.055	7.997	7.792	7.843	7.808	7.698	7.754	7.758	7.800	7.965	7.865	7.709	7.793	7.760	7.862	7.833
Al_{iv}	0.000	0.000	0.000	0.003	0.208	0.095	0.096	0.302	0.246	0.218	0.147	0.035	0.078	0.291	0.207	0.240	0.138	0.167
Σ	8.14	8.10	8.06	8.00	8.00	7.94	7.90	8.00	8.00	7.98	7.95	8.00	7.94	8.00	8.00	8.00	8.00	8.00
Al_{vi}	0.074	0.077	0.196	0.169	0.000	0.000	0.000	0.040	0.020	0.000	0.000	0.015	0.000	0.003	0.010	0.016	0.007	0.031
Ti	0.011	0.013	-----	0.054	0.017	0.005	0.005	0.019	0.029	0.022	0.010	0.032	0.012	0.017	0.020	0.018	0.011	0.010
Fe^{3+}	0.632	0.621	1.495	1.585	1.194	1.112	1.432	1.157	1.127	1.313	1.242	1.752	-----	1.291	1.204	1.224	1.026	1.152
Fe^{2+}	0.591	0.682	1.006	0.787	0.336	0.177	0.084	0.272	0.355	0.164	0.165	0.698	2.355	0.191	0.365	0.356	0.172	0.166
Mn	-----	-----	0.017	0.011	0.023	0.049	0.054	0.016	0.023	0.014	0.022	0.007	0.038	0.027	0.022	0.018	0.029	0.018
Mg	3.558	3.511	2.186	2.394	3.431	3.719	3.521	3.497	3.447	3.510	3.614	2.497	4.576	3.471	3.380	3.368	3.755	3.624
Σ	4.87	4.90	4.90	5.00	5.00	5.06	5.10	5.00	5.00	5.02	5.05	5.00	6.98	5.00	5.00	5.00	5.00	5.00
Ca	0.079	0.053	0.349	0.066	0.180	0.297	0.163	0.165	0.212	0.297	0.142	0.017	0.075	0.253	0.240	0.202	0.117	0.464
Na	2.407	2.538	1.538	1.941	2.352	2.207	2.233	2.357	2.332	2.035	2.371	2.119	0.136	2.173	2.204	2.290	2.311	1.833
K	0.438	0.439	0.052	0.069	0.270	0.295	0.287	0.379	0.285	0.279	0.337	0.052	0.035	0.284	0.271	0.270	0.537	0.203
Σ	2.92	3.03	1.94	2.08	2.80	2.80	2.68	2.90	2.83	2.61	2.85	2.19	0.25	2.71	2.71	2.76	2.97	2.50
F	---	---	---	0.3	1.5	1.2	1.2	1.1	0.9	0.9	1.0	0.1	0.05	0.9	1.1	1.1	1.2	0.6

Iron oxides were resolved in formulae calculations, except in 017 and 250b. All analyses were carried out by electron microprobe, except for amphibole 017, which was analyzed by standard chemical procedures. n.a. not analyzed.

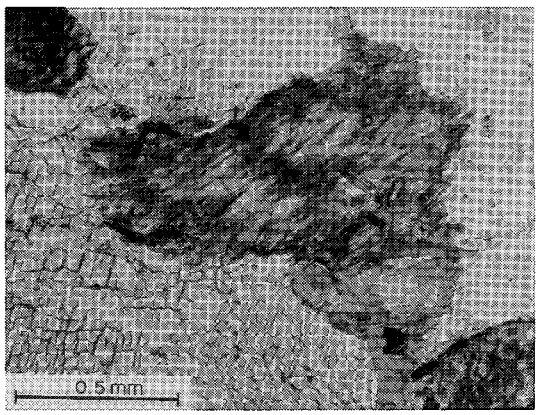

FIG. 5. Large, polygranular cluster of amphibole (centre of photograph) in microcline. Cummingtonite (light grey) is replaced on the exterior of the cluster and along fractures by magnesio-riebeckite (dark grey). Plane-polarized light, thin section 250.

a plot involving *A* and *B* cations (lines *MA* and *MR*, Fig. 6), where *A* and *B* refer to the general formula for amphibole $AB_2C_5T_8O_{22}(OH)_2$ (model 1).

As an alternative, model 2, magnesio-arfvedsonite and magnesio-riebeckite can be fitted (less closely) to winchite – magnesio-arfvedsonite and winchite – magnesio-riebeckite joins, requiring substitutions of the type $\square + Ca \rightarrow Na + Na$ and $Ca + Mg \rightarrow Na + Fe^{3+}$, respectively. Zoning relationships suggest that Na-amphibole becomes depleted in calcium during growth, and the two curves of model 1 are, therefore, curves of paragenetic order. According to model 1, during mineral development vacant sites ($\square$) are progressively filled. In model 2, vacant sites in magnesio-arfvedsonite become filled but their proportion in magnesio-riebeckite remains constant.

In both amphibole and pyroxene, the four principal variables Fe, Mg, Ca and Na + K can be evaluated on a Fe† – Ca† diagram [Fig. 7; Fe† = $100Fe_T/(Fe + Mg)$, Ca† = $100Ca/(Ca + Na + K)$]. Early pyroxene compositions, with high Ca†, deviate from the dotted line (slope Ca†/Fe† = −1) but become coincident with it at lower Ca† values. This can be explained by oxidation of iron in high-Ca† compositions according to a hedenbergite → aegirine substitution ($Ca + Fe^{2+} \rightarrow Na + Fe^{3+}$). To explain the departure from a vertical line, we propose a concomitant diopside → aegirine substitution ($Ca + Mg \rightarrow Na + Fe^{3+}$). These substitutions proceed down to about Ca† = 10, at which point all the available iron is completely oxidized. From there, substitution is diopside → aegirine. The deviation from the diopside–aegirine line at high Ca† can also be explained in terms of vacant octahedral sites. However, we prefer the first alternative; it conforms with a major period of oxidation, as evident from the observations of the oxide assemblage by Cockburn (1966) and with the chemical composition of aegirine in similar deposits elsewhere (see below).

On the other hand, the plots of specimens 005 and 006, analyzed wet-chemically, cannot be explained in this manner. Ca† is too high with respect to Fe†, and the ions Ca^{2+} and Mg^{2+} have not been

TABLE 3. CHEMICAL COMPOSITION OF PYROXENE

	001	002	005	006	009	041	062	113	114c	114r	126
SiO_2	52.67	53.10	51.65	51.69	52.57	53.88	52.99	52.56	52.71	53.19	52.79
TiO_2	0.18	0.13	0.042	0.068	0.05	0.07	1.63	0.35	0.30	0.32	0.26
Al_2O_3	2.91	1.98	3.14	2.26	2.37	0.92	0.38	0.71	1.14	1.59	1.19
Cr_2O_3	n.a.	0.06	n.a	n.a.	n.a.	n.a.	n.a.	0.03	n.a.	n.a.	n.a.
Fe_2O_3	32.06	30.16	31.05	31.60	31.92	29.70	29.55	30.70	31.33	31.30	31.65
FeO	0.34	0.91	0.24	0.29	0.00	0.35	0.00	0.00	0.00	0.43	0.11
MnO	n.a.	0.08	<0.002	<0.002	n.a.	0.05	0.05	0.09	0.11	0.12	0.08
MgO	0.25	0.17	0.03	0.10	0.24	2.24	1.46	1.17	1.23	0.74	0.89
CaO	0.34	0.30	0.94	0.98	0.19	3.23	2.20	1.95	1.86	1.31	1.44
Na_2O	13.11	13.33	13.14	13.04	14.17	11.43	12.95	12.97	13.10	13.00	12.87
K_2O	0.37	0.04	<0.02	<0.03	0.01	0.03	0.04	0.02	0.00	0.02	0.02
H_2O	n.a.	n.a.	<0.05	<0.05	n.a.	n.a.	n.a.	n.a.	n.a.	n.a.	n.a.
Total	102.23	100.26	100.30	100.11	101.52	101.90	101.25	100.37	101.78	102.02	101.30
Ions based on 4 cations and 6 oxygens											
Si	1.964	2.011	1.962	1.973	1.957	1.997	1.988	1.993	1.967	1.987	1.988
Al_{iv}	0.936	0.000	0.038	0.027	0.043	0.003	0.012	0.007	0.033	0.013	0.012
Σ	2.00	2.01	2.00	2.00	2.00	2.00	2.00	2.00	2.00	2.00	2.00
Al_{vi}	0.092	0.088	0.103	0.075	0.061	0.037	0.005	0.025	0.017	0.057	0.041
Ti	0.005	0.004	0.001	0.002	0.001	0.002	0.046	0.010	0.008	0.009	0.007
Cr	-----	0.002	-----	-----	-----	-----	-----	0.001	-----	-----	-----
Fe^{3+}	0.900	0.860	0.888	0.908	0.894	0.829	0.834	0.876	0.880	0.880	0.897
Fe^{2+}	0.011	0.029	0.008	0.009	0.000	0.011	0.000	0.000	0.000	0.014	0.003
Mn	-----	0.003	0.000	0.000	-----	0.002	0.002	0.003	0.003	0.004	0.003
Mg	0.014	0.010	0.002	0.016	0.013	0.124	0.082	0.066	0.068	0.041	0.050
Σ	1.02	1.00	1.00	1.00	0.97	1.00	0.97	0.98	0.98	1.00	1.00
Ca	0.014	0.012	0.038	0.040	0.008	0.128	0.088	0.079	0.074	0.052	0.058
Na	0.948	0.979	0.968	0.965	1.023	0.866	0.942	0.940	0.948	0.942	0.940
K	0.018	0.002	0.000	0.000	0.000	0.001	0.002	0.001	0.000	0.001	0.001
Σ	0.98	0.99	1.01	1.00	1.03	1.00	1.03	1.02	1.02	1.00	1.00

	127c	127r	176c	176r	248c	248r	263	296c	296r	300	305
SiO_2	52.79	52.08	51.93	52.74	52.89	52.41	52.85	52.61	52.49	52.55	53.15
TiO_2	0.32	0.42	0.51	0.11	0.46	0.39	0.11	0.31	0.32	0.58	0.39
Al_2O_3	1.37	1.43	1.06	0.06	0.67	1.07	0.16	0.48	1.00	0.59	0.92
Cr_2O_3	n.a.	n.a.	n.a.	n.a.	n.a.	n.a.	n.a.	n.a.	n.a.	n.a.	n.a.
Fe_2O_3	29.14	30.87	29.81	32.71	31.34	31.94	24.76	30.06	31.51	30.20	24.92
FeO	1.95	0.80	0.00	0.41	0.23	0.00	4.84	0.06	0.89	1.35	2.91
MnO	0.05	0.04	0.10	0.06	0.10	0.08	0.11	0.09	0.09	0.08	0.18
MgO	0.49	0.38	1.64	0.25	1.51	1.07	2.56	0.93	0.89	0.54	3.20
CaO	0.54	0.39	2.29	0.33	2.16	1.53	4.82	1.32	1.28	0.74	5.18
Na_2O	12.90	13.07	12.42	13.32	12.46	12.85	10.24	12.86	13.17	12.93	10.44
K_2O	0.01	0.01	0.03	0.02	0.03	0.03	0.04	0.02	0.02	0.02	0.02
H_2O	n.a	n.a.	n.a.	n.a.	n.a.	n.a.	n.a.	n.a.	n.a.	n.a.	n.a.
Total	99.56	99.49	99.79	100.01	101.85	101.37	100.49	98.74	101.66	99.58	101.31
Ions based on 4 cations and 6 oxygens											
Si	2.019	1.996	1.976	2.019	1.983	1.973	2.018	1.996	1.982	2.015	1.997
Al_{iv}	0.000	0.004	0.024	0.000	0.017	0.027	0.000	0.004	0.018	0.000	0.003
Σ	2.02	2.00	2.00	2.02	2.00	2.00	2.02	2.00	2.00	2.02	2.00
Al_{vi}	0.062	0.061	0.024	0.003	0.013	0.020	0.007	0.017	0.027	0.027	0.038
Ti	0.009	0.012	0.015	0.003	0.013	0.011	0.003	0.009	0.009	0.017	0.011
Cr	----	----	----	----	----	----	----	----	----	----	----
Fe^{3+}	0.839	0.890	0.854	0.942	0.885	0.905	0.711	0.915	0.895	0.872	0.705
Fe^{2+}	0.062	0.026	0.000	0.013	0.007	0.000	0.155	0.002	0.000	0.043	0.092
Mn	0.002	0.001	0.003	0.002	0.003	0.003	0.004	0.003	0.003	0.003	0.006
Mg	0.028	0.022	0.093	0.014	0.084	0.060	0.146	0.053	0.050	0.030	0.179
Σ	1.00	1.01	0.99	0.98	1.01	1.00	1.03	1.00	0.98	0.99	1.03
Ca	0.022	0.016	0.093	0.014	0.087	0.062	0.197	0.054	0.052	0.030	0.209
Na	0.957	0.971	0.916	0.989	0.906	0.938	0.758	0.946	0.964	0.961	0.761
K	0.000	0.000	0.001	0.001	0.001	0.001	0.002	0.001	0.001	0.001	0.001
Σ	0.98	0.99	1.01	1.00	0.99	1.00	0.96	1.00	1.02	0.99	0.97

Iron oxides resolved in formulae calculations, except in 005 and 006. All analyses by electron microprobe except 005 and 006 (which were made by standard chemical procedures). n.a. = not analysed.

substituted equally, as stipulated by the diopside → aegirine model. Ca-rich aegirine occurs in late calcite–aegirine veinlets and perhaps formed under different conditions from pyroxene compositions of the main trend.

Specimen 127 contains a sharply terminated, zoned euhedral aegirine crystal, lying at the contact of two hematite grains containing oriented intergrowths of rutile. This suggests that aegirine + hematite (± rutile) or, if hematite is secondary, aegirine + one or more primary oxides of Fe and Ti formed contemporaneously.

Most magnesio-arfvedsonite compositions define a smooth curve on the left-hand side of Figure 7, but the compositions of three specimens (017, 062 and 250) lie well beyond this line and can be fitted to a subsidiary, parallel, magnesio-riebeckite curve. We suggest that magnesio-arfvedsonite formed by

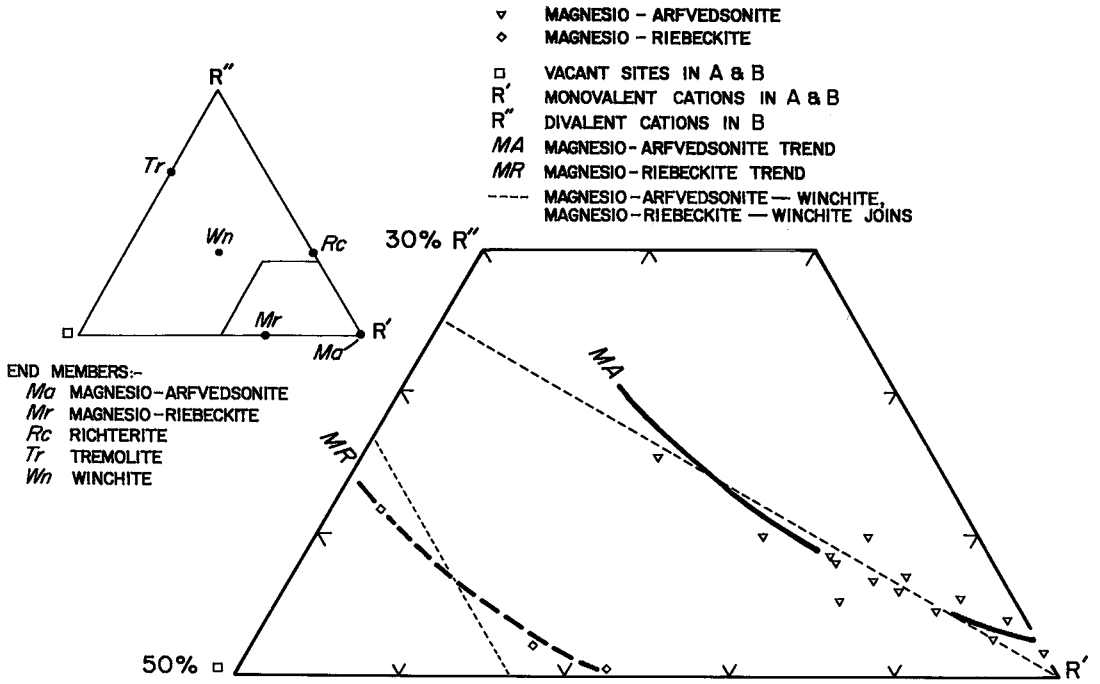

FIG. 6. The Na-amphibole compositions from Cantley plotted with respct to monovalent cations R′, divalent cations R″, and vacancies □ in the *A* and *B* positions of the formula $AB_2C_5T_8O_{22}(OH,F)_2$, showing the two lineages and trends of mineral development.

replacement of the dominant biotite gneiss, where K and F were plentiful. In contrast, we believe that magnesio-riebeckite formed from a two-pyroxene gneiss, which is particularly abundant in the areas that furnished specimens 017 and 062. Specimen 250 contains 5% cummingtonite (Table 3, composition 250*b*) pseudomorphous after hypersthene, as well as rare, relict hypersthene. Magnesio-riebeckite appears to replace cummingtonite in preference to hypersthene. Kushev (1960, 1961) and Lazarenko (1977) have shown that at Krivoi Rog, U.S.S.R., magnesio-riebeckite, not magnesio-arfvedsonite, is derived from cummingtonite by alkali metasomatism.

Little can be said about the paragenetic relationships of aegirine to magnesio-riebeckite on the basis of one specimen (062). Amphibole and pyroxene are, apparently, not in contact and, therefore, textural evidence is lacking.

Pyroxene compositions can be linked to coexisting magnesio-arfvedsonite with a series of tie lines. Thus according to textural evidence, the three lowest tie-lines of Figure 7 may connect coeval pairs. In contrast, a post-pyroxene amphibole characterizes specimen 263, and its tie line cannot link a pair in equilibrium. In constructing these tie lines the core of zoned pyroxene was assumed to be in equilibrium with the core of an associated zoned amphibole, but this is probably true to a first approximation only.

Similarly, the pyriboles can be plotted on a Na – Ca – K diagram (Fig. 8). Most tie lines that link pairs of coexisting amphibole and pyroxene fan out from magnesio-arfvedsonite to aegirine. Throughout the early and middle stages of magnesio-arfvedsonite development, corresponding to the lowest to intermediate content of Na (and, possibly, throughout the whole episode of magnesio-riebeckite formation), K remains approximately constant, but appears to increase in the late, or high-Na stage. No trends of pyribole compositions are evident along or across the general strike or across the main Haycock deposit from which four pyribole specimens (001, 002, 062, 009) were collected.

NONIGNEOUS ALKALI PYRIBOLES

The Cantley pyriboles can be compared with others from isochemically and metasomatically derived rocks using the following examples: (1) *Metaevaporite (isochemically derived rock),* from the Grabenbach – Grundlsee – Rigaus region, near Salzburg, Austria (Kirchner 1980), (2) *fenite derived from carbonatite (metasomatic rock),* with paleoliths of amphibolite and granite, from Sokli, Finland

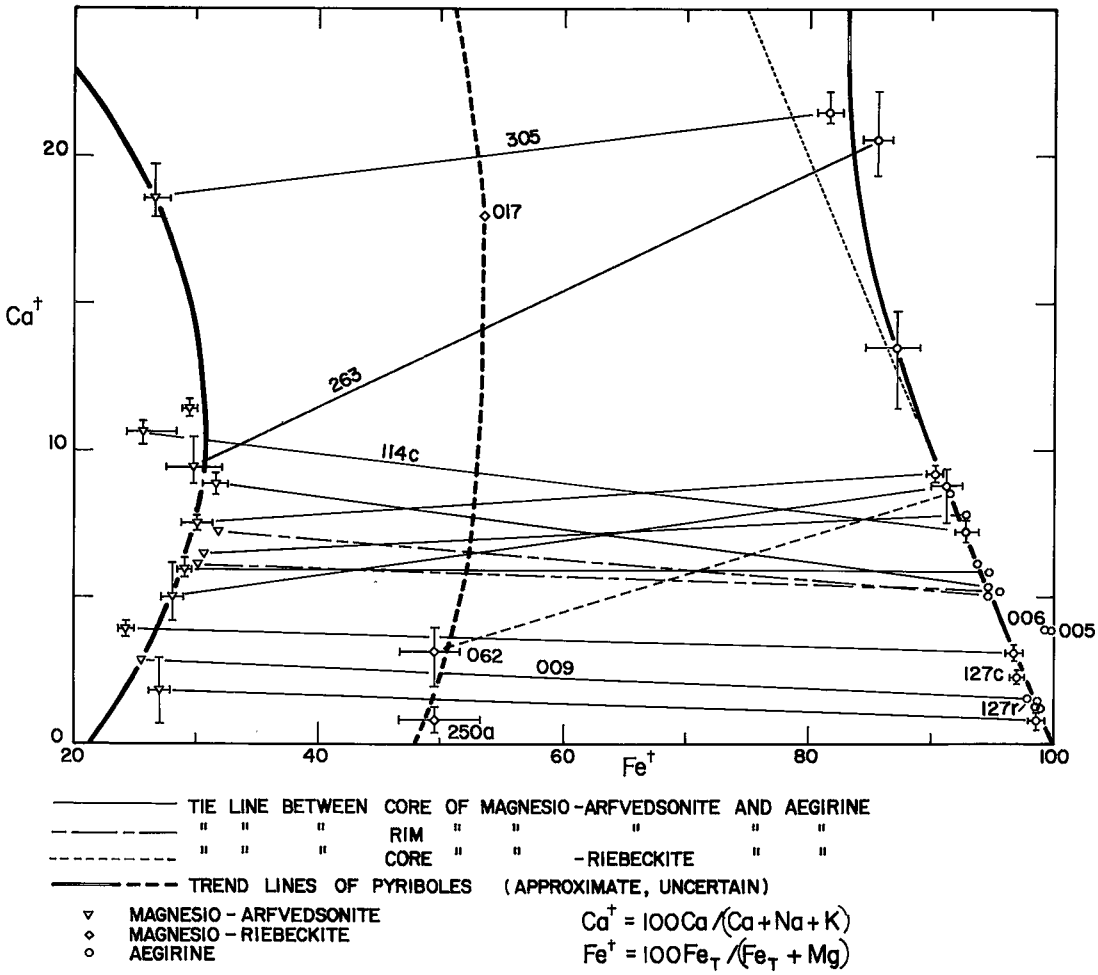

FIG. 7. The Cantley pyriboles are plotted with respect to 100 Ca/(Ca+Na+K) (= Ca†) and 100 $Fe_T/(Fe_T + Mg)$ (= Fe†), showing tie lines between associated pairs (same thin section), lineages, and evolutionary trends. Error bars indicate precision of microprobe analyses.

(Vartiainen & Woolley 1976, Vartiainen 1980). Additional data from other sources will be quoted on captions to the appropriate diagrams. (3) *Nonigneous rock of disputed origin,* from Krivoi Rog, U.S.S.R. (Nikol'skii 1961, Kushev 1960, 1961, Polovko 1970). This may have been metasomatically derived by solutions from granitic rock which replaced jaspilite (as proposed by Eliseev & Nikol'skii 1961, Polovko 1970), or formed through isochemical transformations in an Fe- and Na-rich protolith (as proposed by Aleksandrov 1962, 1963, Lazarenko 1977).

Grains of fenitic pyroxene commonly show zoning with a more augitic core and more aegirinic rim (Sergeev 1967, Sutherland 1969), indicating a progressive increase in Na (and decrease in Ca†) with mineral development. Similar zonation has been noted in pyroxenes of "metasomatites" of the Krivoi Rog (Nikol'skii 1961, Eliseev & Nikol'skii 1961) and in amphiboles from fenites around alkaline complexes of the Kola Peninsula (Sergeev 1967). These features conform with mineral zoning in the Cantley pyriboles and suggest that paragenetic trends should be investigated on diagrams of the type used here (Figs. 6, 7 and 8).

Fenitic amphiboles, especially those of Sokli, lack vacancies in the *A* position, and the trend becomes linear along R′ – R″ (Fig. 9). On the same diagram, the Salzburg amphiboles cluster around *Mr.* The Krivoi Rog data-points are widely scattered, extending from close to *Ma* ($A + B_{max} = 2.60$) to beyond *Mr,* with a clustering around *Mr.* More significant is their position on the Ca† – Fe† diagram (Fig. 10).

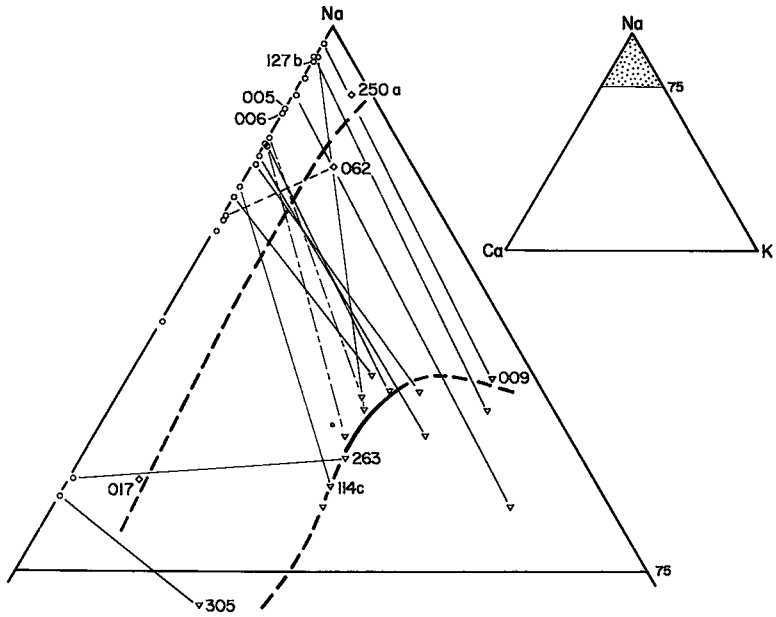

FIG. 8. Na–Ca–K diagram of Cantley pyriboles, showing tie lines between associated pairs, the three lineages and evolutionary trends. Symbols as in Figure 7.

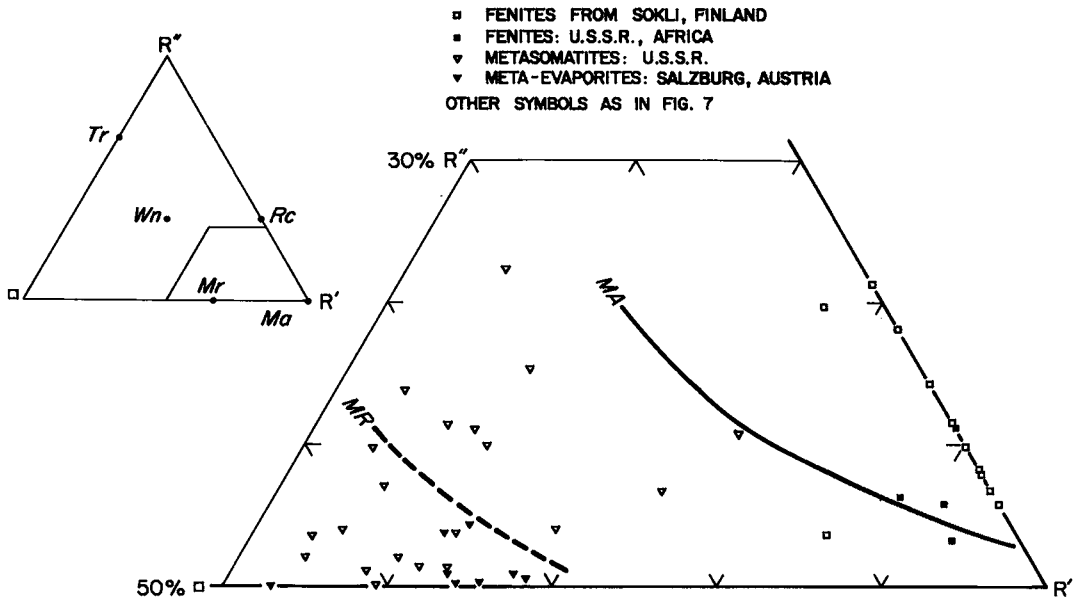

FIG. 9. R′–R″–□ diagram (*cf.* Fig. 6) showing plots of Na-amphibole from deposits of three types: fenites associated with carbonatite (data from McKie 1966, Sutherland 1969, Vartiainen & Woolley 1976, Vartiainen 1980, Secher & Larsen 1980), "metasomatites" associated with granite (Kushev 1961, Glagolev 1966), and meta-evaporites (Kirchner 1980). The trends defined by the Cantley amphiboles have been added for comparison.

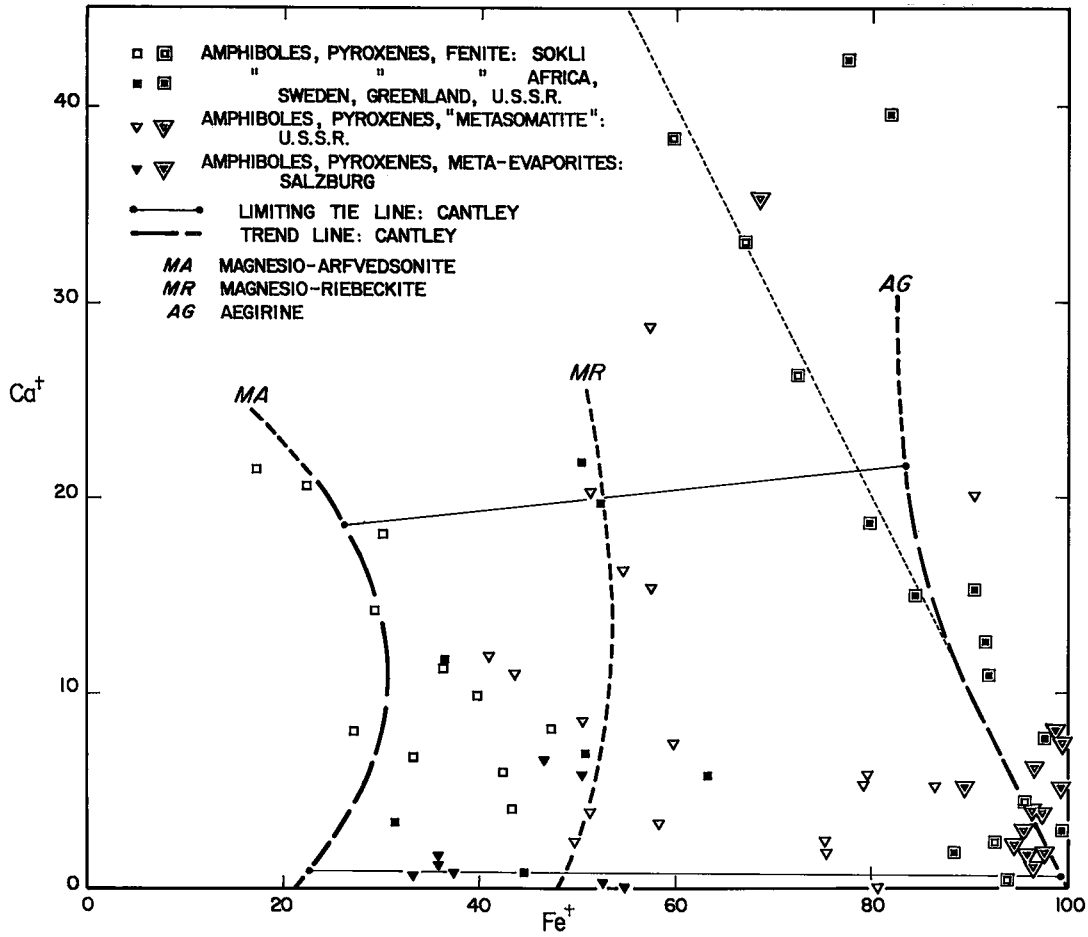

FIG. 10. Ca† - Fe† diagram (*cf.* Fig. 7) for Na-pyriboles for the three types of occurrence shown in Figure 9, with trend lines and limiting tie-lines of the Cantley pyriboles added for comparison. Data from von Eckermann (1966), Sergeev (1967) and Kulakov *et al.* (1974) have been added to those used in Figure 9.

At high Ca†, fenitic amphiboles plot close to the Cantley magnesio-riebeckite trend, but depart from this curve at low Ca†, whence they become enriched in Fe. A similar trend can be seen in pyroxenes, where Fe† is increased as Ca† is depleted in the approximate ratio 1:1 (owing to complex replacements involving Fe^{2+}, Fe^{3+}, ^{iv}Al, Ti, Mg, Ca and Na). The Salzburg pyroxenes plot close to magnesio-riebeckite. Pyroxene compositions from the Krivoi Rog rocks cluster around pure aegirine, but the plots of associated amphiboles show wide scatter. According to Kushev (1960) and Pavlenko (1959), the general trend, from early to late stages of metasomatism, is one of continuous addition of Fe to the amphibole, leading from magnesio-riebeckite, to riebeckite but irregularities appear through variations in the composition of the paleosome (cummingtonite-grunerite).

On the Na–Ca–K diagram (Fig. 11), the majority of compositions of amphibole from Sokli defines a linear trend between the Cantley magnesio-riebeckite line (upper trend) and the Cantley magnesio-arfvedsonite line (lower trend). The other plots of fenitic amphibole are dispersed. The Salzburg data-points cluster around the Na apex and are K-depleted; the Krivoi Rog data-points are widely dispersed but show a tendency to depletion in K.

Tie lines between associated pyroxene and amphibole in fenites intersect each other and intersect tie lines linking pyriboles of the Cantley fenites. For simplicity, they have been omitted from the diagrams. Unfortunately, it is impossible to define

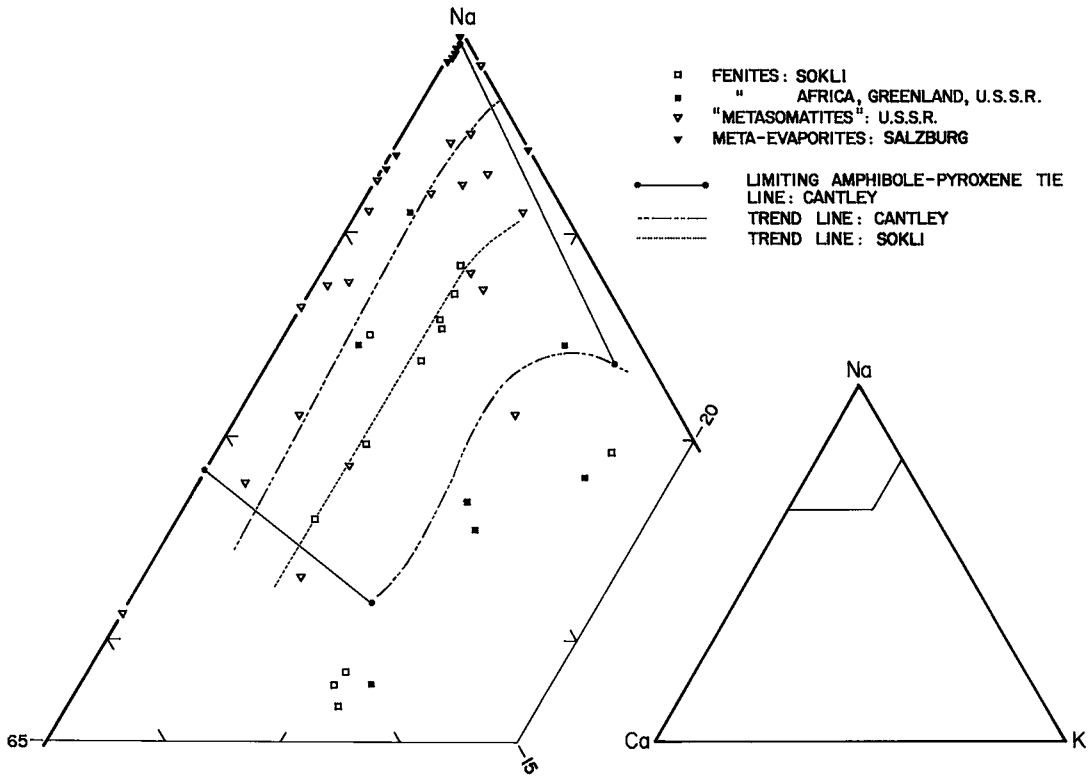

FIG. 11. Na - Ca - K diagram (*cf.* Fig. 8) for Na-(Mg-)amphibole from the three types of occurrence shown in Figure 9, with trend lines and limiting tie-lines defined by the Cantley pyriboles added for comparison.

associated amphibole - pyroxene pairs at Krivoi Rog and Salzburg from the published data. Also not shown on our diagrams is Al, which is notably high in the Salzburg pyriboles, intermediate in the Sokli pyriboles, low in the Cantley pyriboles, and extremely variable in the Krivoi Rog pyriboles.

Pyriboles in meta-evaporite are chemically distinct from those in fenite. The former cluster on variation diagrams, as would be expected in a closed system. On the other hand, pyriboles from fenite tend to follow smooth curves on these diagrams, which seems natural for an open system with continuous readjustment of composition of the starting material to changing P-T-X conditions. The chemical composition of the starting material is also important, so that pyriboles from both metasomatic rocks and meta-evaporites will vary somewhat from one occurrence to the next and even within an individual occurrence. These controls explain the well-defined chemical trends of fenitic pyriboles in the Cantley region outlined in Figure 1, a small area with minor variations in the protoliths. Violations of these controls may partly account for the scatter of pyribole compositions at Sokli, where fenite consists of both altered granite and amphibolite. Vartiainen & Woolley (1976) contended that location of a fenitic pyribole with respect to a large carbonatite intrusion (a T-X control) is also important, and that, at Sokli, pyriboles from fenite close to the carbonatite are higher in Ca than those from fenite further away. This effect is impossible to evaluate for specimens from Cantley, where large bodies of carbonatite are absent.

The Krivoi Rog rocks, with pyriboles of dubious parentage, do not fit either metasomatic or isochemical models of origin. Specimens were derived from an area of considerable size (a strip 40 km long, 1-3 km wide); variations in the protolith are known to occur (Nikol'skii & Eliseev 1961), which would account for the scatter in variation diagrams using either model.

OXIDATION

The degree of oxidation of pyriboles can be expressed in terms of $Fe^{3+}/(Fe^{3+}+Fe^{2+})$ or oxidation ratio (O.R.); this function can be plotted against Ca† as in Figure 12. Our amphibole compositions (Fe^{2+}

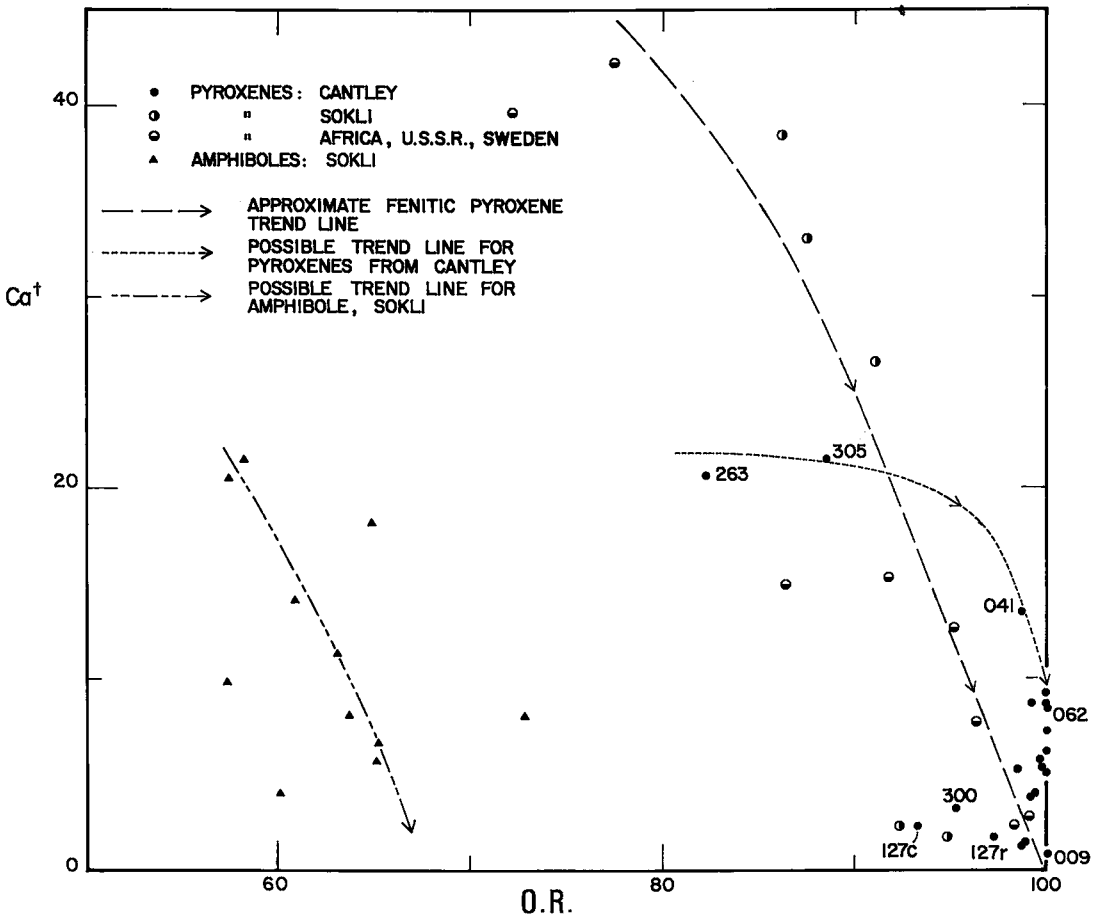

FIG. 12. Ca† – O.R. diagram [O.R. = 100 $Fe^{3+}/(Fe^{2+} + Fe^{3+})$] showing approximate oxidation trend of pyroxene compositions from carbonatite-linked fenites, a possible trend of the Cantley pyroxenes and the field of Sokli (Finland) amphiboles. Compositional data for pyroxene from von Eckermann (1966), McKie (1966), Sergeev (1967), Sutherland (1969), Kulakov *et al.* (1974), Vartiainen & Woolley (1976), and Table 3 (this paper); data for Sokli amphiboles from Vartiainen & Woolley (1976).

and Fe^{3+} calculated) give scattered oxidation ratios (not plotted) but values are consistently lower than those of pyroxene. Amphibole and pyroxene from the Krivoi Rog region (Fe^{2+} and Fe^{3+} determined chemically) also give scattered plots. All but one of the pyribole compositions from the Salzburg metaevaporites (Kirchner 1980) are derived from microprobe analyses. For simplicity, we plot compositions of fenitic pyroxene and of amphibole from Sokli and compare their trends with plots of O.R. calculated for pyroxene compositions from Cantley (Fig. 12).

Fenitic pyroxenes from Finland (Sokli), Sweden (Alnö) and various localities in U.S.S.R. and Africa show a trend of gradual oxidation from early (high Ca†) aegirine-augite to later aegirine. A trend is also suggested through the Sokli amphibole field.

Progressive oxidation is also suggested in the Cantley pyroxene but with a different trend. Early pyroxene underwent intense oxidation, becoming completely oxidized at about Ca† 10. This oxidation conforms with the occurrence of partially martitized magnetite associated with pyriboles of the intermediate stage (*e.g.*, specimen 041). Hematite is the only iron oxide associated with pyriboles of the late stage (*e.g.*, specimen 009).

A check on the oxidation ratio was made by Mössbauer analysis for a sample collected close to the source of specimen 062 (adit portal, Haycock mine). Measured and calculated O.R. values are in good agreement: O.R. of pyroxene by Mössbauer spectroscopy ≈ 100, by calculation from the

analytical data 100; O.R. of amphibole by Mössbauer spectroscopy 68.0, by calculation from the analytical data 66.8.

Conclusions

Chemical compositions of pyriboles from Cantley are similar to those of Sokli and other occurrences where fenites have been derived from carbonatite. Differences in mineral chemistry and mineral development can possibly be explained in terms of variations in host rock and different physicochemical conditions of mineral formation. The Cantley pyribole suite occurs in a particular biotite gneiss horizon and, therefore, the host rock is compositionally rather uniform. Less common hypersthene + diopside + plagioclase gneiss appears to give rise to magnesio-riebeckite instead of magnesio-arfvedsonite.

We propose that Na, K, Mg and, perhaps, other elements, were introduced by carbonatites near Cantley, on the north side of the Ottawa - Bonnechère graben, under conditions of waning thermal activity, near the close of Grenvillian metamorphism (*ca.* 950 Ma b.p.). The resulting fenitization was accompanied by progressive oxidation. We further suggest that the calcium-depletion trend in pyriboles corresponds to deposition during falling temperature, as proposed for similar changes in pyriboles in fenites derived from carbonatites in the Kola Peninsula by Sergeev (1967).

Acknowledgements

The authors acknowledge an NSERC grant (A2122), which defrayed research costs. The final work was done at the Smithsonian Institution and the U.S. Geological Survey (Reston, Va.) by Hogarth while on sabbatical leave. Mössbauer analyses were made under the supervision of Michael Townsend at the Mines Branch (now CANMET), Ottawa and aegirine specimens 005 and 006 were separated at the University of Ottawa by Ann Hobart Kasowski. We thank the following persons for reviewing the manuscript and providing helpful comments for its improvement: Daniel Appleman (Smithsonian Institution), Michael Fleischer, E-an Zen and Jane Hammarstrom (U.S. Geological Survey), John Moore, (Carleton University), Ralph Kretz (University of Ottawa) and two anonymous referees. Diagrams were drawn and photomicrographs taken by Edward Hearn (University of Ottawa) and the manuscript was typed by Carole Brown and Kathy Ledger.

References

Albee, A.L. & Ray, L. (1970): Correction factors for electron probe microanalysis of silicates, oxides, carbonates, phosphates and sulfates. *Anal. Chem.* **42,** 1408-1414.

Aleksandrov, I.V. (1962): Sodium metasomatism occurring in the Krivoi Rog area. *In* Tr. Shestogo Soveshch. po Eksperim. i Tekhn. Mineral. i Petrogr. (A.I. Tsvetkov, ed.). *Akad. Nauk S.S.S.R., Inst. Khim. Silikatov* **1961,** 61-66 (in Russ.).

_____ (1963): Sodic metasomatism in the Krivoi Rog area. *In* Geokhimiya Shchelochnogo Metasomatoza (V.V. Shcherbina, ed.). *Akad. Nauk S.S.S.R., Inst. Geokhim. Anal. Khim.* **1963,** 74-151 (in Russ.).

Bence, A.E. & Albee, A.L. (1968): Empirical correction factors for the electron microanalysis of silicates and oxides. *J. Geol.* **76,** 382-403.

Cirkel, F. (1909): Report on the iron ore deposits along the Ottawa (Quebec side) and Gatineau Rivers. *Canada Mines Br., Publ.* **23.**

Cockburn, G.H. (1966): *Geology of the Haycock Mine, Gatineau Area, Quebec.* B.Sc. thesis, Univ. Ottawa, Ottawa, Ontario.

Deer, W.A., Howie, R.A. & Zussman, J. (1978): *Rock-Forming Minerals. 2A. Single-Chain Silicates.* Longmans, Green and Co., London.

von Eckermann, H. (1966): The pyroxenes of the Alnö carbonatite (sövite) and of the surrounding fenites. *Mineral. Soc. India, IMA vol.,* 126-139.

Eliseev, N.A. & Nikol'skii, A.P. (1961): Types of metasomatites, their relation, and genesis. *Tr. Lab. Geol. Dokembriya, Akad. Nauk S.S.S.R.* **13,** 172-197 (in Russ.).

Gittins, J., Macintyre, R.M. & York, D. (1967): The ages of carbonatite complexes in eastern Canada. *Can. J. Earth Sci.* **4,** 651-655.

Glagolev, A.A. (1966): *Metamorphism of Precambrian Rocks of the Kursk Magnetic Anomaly. Petrography and Mechanisms of Metamorphism of Iron Formation and Certain Other Precambrian Rocks of the Ancient Slice in the Iron Ore Region of the Kursk Magnetic Anomaly.* Izd. Nauka, Moscow (in Russ.).

Hogarth, D.D. (1966): Intrusive carbonate rock near Ottawa, Canada. *Mineral. Soc. India, IMA vol.,* 45-53.

_____ (1977): Iron-alkali mineralization near Cantley, Quebec. *Geol. Assoc. Can. - Mineral. Assoc. Can. Program Abstr.* **2,** 25.

_____ (1981): Géologie de la partie ouest de la région de Quinnville. *Ministère de l'énergie et des ressources du Québec, Rapport intérimaire* **DPV-816.**

_____ & Moore, J.M. (1972): Excursion stops in Precambrian rocks. 6. The Haycock property. *In* Geology of the National Capital area. (D.M. Baird, ed.). *24th Int. Geol. Congr. (Montreal), Guidebook to Excursions* **B23–B27.**

JEN, LO-SUN (1973): The determination of iron(II) in silicate rocks and minerals. *Anal. Chim. Acta* **66**, 315-318.

KIRCHNER, E.C. (1980): Natriumamphibole und Natriumpyroxene als Mineralneubildungen in Sedimenten und basischen Vulkaniten aus dem Permoskyth der Nordlichen Kalkapen. *Geol. Bundesanst (Wein) Verh.*, 249-279.

KULAKOV, A.N., EVDOKIMOV, M.D. & BULAKH, A.G. (1974): Mineral veins in fenites of the Tur'ii Peninsula in the Murmansk region. *Zap. Vses. Mineral. Obshchest.* **103**, 179-191 (in Russ.).

KUSHEV, V.G. (1960): Alkaline amphiboles of Krivoi Rog. *Tr. Lab. Geol. Dokembriya, Akad. Nauk S.S.S.R.* **11**, 278-291 (in Russ.).

_____ (1961): Alkaline amphiboles in the Krivoi Rog metasomatites. *Tr. Lab. Geol. Dokembriya, Akad. Nauk S.S.S.R.* **13**, 44-51 (in Russ.).

LAPOINTE P. (1979): *Fenitization around Hematite Occurrences at the Haycock Mine, Hull and Templeton Townships, Quebec.* M.Sc. thesis, Univ. Ottawa, Ottawa, Ontario.

LAZARENKO, E.K. (1977): *Mineralogy of the Krivoi Rog Basin.* Naukova Dumka, Kiev (in Russ., Eng. summ.).

LEAKE, B.E. (1978): Nomenclature of amphiboles. *Can. Mineral.* **16**, 501-520.

LUMBERS, S.B. (1982): Summary of metallogeny, Renfrew County area. *Ont. Geol. Surv. Rep.* **212.**

MCKIE, D. (1966): Fenitization. *In* Carbonatites (O.F. Tuttle & J. Gittins, eds.). John Wiley & Sons, New York.

NIKOL'SKII, A.P. (1961): Aegirines and aegirine-augites in the Krivoi Rog metasomatites. *Tr. Lab. Geol. Dokembriya, Akad. Nauk S.S.S.R.* **13**, 26-44 (in Russ.).

_____ & ELISEEV, N.A. (1961): General information on metasomatites of the Krivoi Rog ore belt. *Tr. Lab. Geol. Dokembriya, Akad. Nauk S.S.S.R.* **13**, 18-25 (in Russ.).

PAVLENKO, A.S. (1959): Peculiarities of metasomatism in a region of northern Krivoi Rog area. *Izvest. Akad. Nauk S.S.S.R., Ser. Geol.* **1959** (no. 1), 81-101 (in Russ.).

POLOVKO, N.I. (1970): *Material Balance During the Formation of Alkaline Metasomatites of the Krivoi Rog Jaspilite Zones.* Izd. Naukova Dumka, Kiev (in Russ.).

RUCKLIDGE, J.C. & GASPARRINI, E.L. (1969): Specifications of a computer program for processing electron microprobe analytical data: EMPADR VII. *Dep. Geol., Univ. Toronto, Toronto, Ont.*

SECHER, K. & LARSEN, L.M. (1980): Geology and mineralogy of the Sarfartôq carbonatite complex, southern west Greenland. *Lithos* **13**, 199-212.

SERGEEV, A.S. (1967): *Fenite Complexes of Ultrabasic and Alkalic Rock.* Leningrad State University, Leningrad (in Russ.).

SUTHERLAND, D.S. (1969): Sodic amphiboles and pyroxenes from fenites in east Africa. *Contr. Mineral. Petrology* **24**, 114-135.

VARTIAINEN, H. (1980): The petrography, mineralogy and petrochemistry of the Sokli carbonatite massif, northern Finland. *Geol. Surv. Finland Bull.* **313.**

_____ & WOOLLEY, A.R. (1976): The petrography, mineralogy and chemistry of the fenites of the Sokli carbonatite intrusion, Finland. *Geol. Surv. Finland Bull.* **280.**

WANLESS, R.K., STEVENS, R.D., LACHANCE, G.R. & DELABIO, R.N. (1974): Age determinations and geological studies. K-Ar isotopic ages, Report 11. *Geol. Surv. Can. Pap.* **73-2.**

Received February 21, 1983, revised manuscript accepted August 16, 1983.